Experimental validation of numerically predicted strain and micromotion in intact and implanted composite hemi-pelvises

Authors and affiliations:

(1) Rajesh Ghosh[1]
(2) Sanjay Gupta[1]
(3) Alexander Dickinson[2]
(4) Martin Browne[2]

[1]Department of Mechanical Engineering, Indian Institute of Technology Kharagpur, Kharagpur 721 302, West Bengal, India.

[2]Bioengineering Science Research Group, School of Engineering Sciences, University of Southampton, Southampton S017 1BJ, United Kingdom.

Corresponding author:

Dr. Sanjay Gupta

Department of Mechanical Engineering

Indian Institute of Technology Kharagpur

Kharagpur 721 302, West Bengal, India

Tel: +91 – (0) 3222 – 282958

Fax: +91 – (0) 3222 – 282277

Email: sangupta@mech.iitkgp.ernet.in

Keywords: pelvis biomechanics, in-vitro testing, strain gauging, implant-bone micro-motion, finite element analysis.

Abstract

The failure mechanisms of acetabular prostheses may be investigated by understanding the changes in load transfer due to implantation, and analysis of the implant-bone micromotion. Computational finite element (FE) models allow detailed mechanical analysis of the implant-bone structure, but their validity must be assessed as part of a verification process before they can be employed in pre-clinical investigations. To this end, in the present study, FE models of composite hemi-pelvises, intact and implanted with an acetabular cup, were experimentally verified. Strains and implant-bone micromotions in the hemi-pelvises were compared with those predicted by the equivalent FE models. Regression analysis indicated close agreement between the measured and FE strains, with a high correlation coefficient (0.95-0.98), a low standard error of the estimate (36-53με) and a low error in regression slope (7-11%). Measured micromotions along three orthogonal directions were small, less than 30μm, whereas the FE predicted values were found to be less than 85μm. Although the trends were similar, the observed deviations may be due to estimation of the interfacial press-fit used in the FE model, and additional artefacts in experimental micromotion measurement which are avoided in the FE model. This supports the FE model as a valid predictor of the experimentally measured strain in the composite pelvis models, confirming its suitability for further computational investigations on acetabular prostheses.

1. Introduction

Loosening of the acetabular prosthesis is responsible for the majority of failures in total hip replacement [1–4]. However, biomechanical investigations into phenomena such as the load transfer mechanism across the pelvis and the acetabular reconstruction remain relatively under-investigated as compared to the femoral component. Measurement of such phenomena across the intact and implanted bones would be a useful step forward in the analysis of acetabular failure, and to date this has commonly been evaluated using finite element (FE) analysis [5–11]. The validity of the FE model generation process should be assessed using quantitative comparisons between computational predictions and experimental results [Anderson et al., 2007].

Researchers have investigated the strain/stress distributions in the intact pelvis by comparing experimentally measured strains with those predicted by the equivalent FE model [5, 7, 10]. However, all these studies featured large areas of rigid fixation, which may not be fully representative of *in-vivo* bone support. Moreover, there is a scarcity of experimental data on strain measurement in intact and implanted pelvises which could be used to identify potential links between changes in strain distribution due to implantation and clinical failure mechanisms [12–14].

The initial fixation of an uncemented implant is dependent on the primary stability, which is usually indicated by the amount of micromotion at the implant-bone interface, prior to bone-ingrowth, induced by the physiological loading conditions during the early post-operative period [15]. Early micromotion, above a range of 50 – 150μm, is believed to be an indicator of future aseptic loosening in cementless hip implants [16–19]. Although some earlier studies were restricted to in-vitro measurement of implant-bone micromotion in the implanted femur [20–23], there have been fewer studies that compared the results with an equivalent FE model of implanted femur [11, 24] and tibia [25]. Despite some published data on the FE predicted acetabular implant-bone micromotion [16, 26–28], to the author's knowledge, there is a dearth of published experimental data on acetabular implant-bone relative displacements. In the present study, an attempt has been made to measure implant-bone micromotion in three orthogonal directions using an artificial composite pelvis and to compare these values with those predicted by the equivalent FE model. The objectives of the present study were: (1) to assess the validity of the generation procedure of the FE models of intact and implanted artificial pelvises, and subsequently, (2) to predict potential biomechanical effects of implantation through a comparison of intact and implanted bone strains and measurement of implant-bone micromotion in implanted composite pelvises.

2. Materials and Methods

The analogue bone model used in this study was a left fourth generation composite pelvis (Sawbones AG, Sweden). This pelvis is composed of foam enclosed with a cortical shell layer made of short glass-fibre reinforced epoxy. This is considered to be a viable alternative to the cadaveric bone for biomechanical evaluation of bone and implant-bone structures [29–37], and represents a standardised geometry of a bone, with gross mechanical behaviour close to that of the human bone. Unlike human cadaveric bones it has very small inter-specimen variability. One pelvis was implanted with a 58 mm outer diameter, 52 mm bearing diameter uncemented acetabular cup (ADEPT®, MatOrtho, UK), following the recommended operative technique. The implant was oriented at 45° inclination and 15° anteversion [28, 38].

2.1 Strain Rosette and LDS fixation

Sets of five rectangular strain rosettes (SR-4® Strain Gauges, Vishay Micro-Measurements, UK) were fixed at pre-determined locations and orientations on the surfaces of the intact and implanted pelvises, along the predominant direction of load transfer, i.e. from the acetabulum to the sacro-iliac joint and pubis symphasis [Dalstra and Huiskes, 1995] (Fig. 1(a)). Since the periacetabular bone is responsible for supporting the implant and would be most affected by implantation, responding by adaptation or fracture, this region is both the most clinically interesting region of the cortical bone, and perhaps the most critical region for validation. The strain rosettes were fixed on flat bone surfaces, which were located at a sufficient distance from the jig constraints and the point of load application to ensure that strains induced in these areas did not interfere with the strains of interest. The bone surface at the strain rosette locations was cleaned with isopropyl alcohol, followed by repeated abrading with 400 grit emery paper and degreasing with water based liquid phosphoric acid, until the surface was smooth. The acid was then neutralized with ammonia water. The rosettes were bonded onto the surface using cyanoacrylate adhesive and connected to a 32-channel strain amplifier (Vishay Micro-Measurements, UK) in a quarter-bridge circuit with internal dummy.

In addition to the strain measurement, three Linear Displacement Sensors (full scale or rated displacement = 5 mm, linearity error = 0.02%) (LDSs, Vishay Micro-Measurements, UK) were mounted on the implanted pelvis to measure implant-bone relative displacements along three orthogonal directions: superior-inferior, anterior-posterior and medial-lateral (Fig. 1). Adjustable links were used to rigidly hold the displacement sensors in desired locations and orientations. One end of a link was mounted on a post, which was rigidly fixed to the bone (Fig.1). The tips of the displacement sensors made contact with a 5 mm square target block, which was welded onto the rim of the implant (Fig.1). The links were used to keep the three LDSs in a desired position and orientation, while ensuring that the tips touched the target block in a direction normal to its surface. The LDSs were also connected to the amplifier. Two successive experiments were carried out to measure surface strains on the intact and implanted pelvises. Subsequently, the implant-bone relative displacements in the implanted pelvis were carried out. Each of these tests was repeated five times, in order to assess measurement repeatability.

2.2 Experimental set-up: fixation and loading of the pelvises

Both intact and implanted composite pelvises were tested on a servo-hydraulic testing machine with a ±25kN load capacity (Instron 8874, Instron Ltd., UK). The pelvises were fixed at two locations, at the sacroiliac joint and posterior to the ilium, and were supported at the pubis (Fig. 2). A proprietary fixture,

developed at the University of Southampton, was used to hold both of the pelvises at an angle such that an axial applied force represented the highest hip joint force in a normal walking cycle, immediately after heel strike [Bergman et al., 2001].

The vertical compressive force was applied on the acetabulum using a 46 mm diameter modular femoral head, connected via a taper to the Instron. Compressive loads were applied at a rate of 14 $Nsec^{-1}$ to a maximum of 200% body weight, 1400 N. The variation of maximum and minimum principal strains with applied load was calculated for each strain rosette using StrainSmart software (Vishay Micro-Measurements, USA). The same test method was used with the implanted pelvis to measure the implant-bone relative displacements at varying load.

2.3 Three-dimensional FE models of the tested composite pelvises

Three dimensional solid geometry of the composite pelvis was obtained from the manufacturer as a CAD model (.sldprt format). The precision of the CAD model was 0.38 mm, according to the specification of the NextEngine 3-D Model 2020i Desktop laser scanner (NextEngine Inc., Santa Monica, NC, USA). The implant and the femoral head were modelled using SolidWorks software (DS SolidWorks Corp., Concord, MA, USA). The solid models of composite pelvis, implant and femoral head were converted into surfaces (.stl format) and imported into Rhinoceros NURBS modelling software (Robert McNeel & Associates, Seattle, USA). Virtual surgery, using Boolean operations was performed after positioning of the cup and femoral head. In the experimental set-up, the distances between five predefined bony landmarks on the pelvis and a location on the modular femoral head (aligned with the vertical axis of the testing machine) were measured. The CAD models of the intact and implanted pelvises were positioned with respect to the CAD model of the vertically oriented femoral head based on these measurements, replicating the orientation of the tested pelvises. Thereafter, the surface models were imported into ANSYS ICEM CFD (ANSYS Inc., PA, USA), in order to generate a volumetric mesh with four-noded tetrahedral elements, with edge lengths varying between 0.5 – 3 mm. The resulting meshes contained ~269,000 and ~285,000 elements for the intact and implanted pelvises respectively. Finally, this volumetric mesh was imported into ANSYS Classic (v11) for the FE analysis, where the elements were converted from first to second order, ten noded tetrahedra, for more accurate solutions.

Linear isotropic elastic homogeneous material properties were used for the foam (E= 155 MPa) and the shell (E= 16.7 GPa), which represent the analogue cancellous and the cortical bone of the composite pelvis, respectively. The Young's Modulus of the acetabular cup and the modular femoral head was taken as 197GPa. The Poisson's ratio for all materials was taken as 0.3. For the intact model, six noded second order asymmetric surface-to-surface contact elements with friction coefficient μ=0.1 were simulated between the acetabular cavity and the modular femoral head. In the implanted composite pelvis, a diametral interference fit of 1 mm was assumed between the rim of the implant and the surrounding bone (57 mm reamed diameter for 58 mm external cup diameter), according to the surgical guidelines for hip resurfacing [26, 28]. At the implant-bone interface, contact elements with μ=0.5 were defined [26, 39]. Frictionless contact was assumed between the modular femoral head and the acetabular component, representing a well lubricated bearing surface. An augmented Lagrangian contact algorithm was used to solve these models [11, 40].

A mesh convergence study was performed by comparing the results between three FE models for both the intact and implanted pelvises [Anderson et al., 2007]. In the intact case, the three models contained 137432, 269376 and 371958 elements. In the implanted case, the three models contained 140147, 284993 and 396615 elements. Comparison between first and the second FE models resulted in

deviations of principal strains and displacements ranging between 2 – 6%. However, the maximum deviation was reduced to 1% when the results of the second and the third models were compared. Therefore, the second set of meshes was deemed sufficiently accurate for the analysis (Fig. 3).

Eight loads were applied to the FE model: 700, 800, 900, 1000, 1100, 1200, 1300, 1400N in order to calculate strains and micromotions. Since the FE models were oriented equivalent to the experimental set-up, these loads were directly applied as quasi-static loads through the modular femoral head for both the tests. Constraints were applied at selected nodes, to simulate fixation of the experimental condition.

In the FE model, the strain corresponding to that recorded by a rosette in the experiment was calculated as the average value of all the surface nodes located underneath the rosette location [11, 41]. This was compared with the strain rosette outputs. In the FE model, the implant-bone relative displacements were calculated as the difference of the displacement values of nodes belonging to the implant surface (area adjacent to square target block welded on implant rim) and nodes belonging to the bone (area adjacent to the cylindrical post rigidly fixed to bone). The correlation coefficient (R), the standard error (SE) of the estimate, linear regression slope (b) and intercept (a), percentage error (PE) in b and test statistic value were used to evaluate whether a significant relationship existed between the measured and numerically predicted data. The PE was calculated as the ratio of SE of b and b. Additionally, the agreement in data was evaluated by the methods outlined by Bland and Altman (1999) and using a concordance correlation coefficient (Lin, 2008). The graphical method of Bland and Altman (1999) evaluates the agreement between the two methods of measurements of the same variable and also gives confidence intervals, using the difference between data obtained by two methods.

3. Results

All strain rosettes and LDSs were found to be active and all measurements were repeatable for all experimental tests: the standard deviation for five repeated loaded data sets for the intact and the implanted pelvis was ± 4.78με and ± 6.1με, respectively. For the measurement of implant-bone relative displacement, the standard deviations (five repeated datasets) along three orthogonal directions were ± 0.2μm (anterior-posterior), ± 1.26μm (superior-inferior) and ± 0.84μm (medial-lateral). An example of typical load-strain curves for the intact and implanted cases (Fig. 4), shows an approximately linear response. The measured and FE predicted strain values of maximum (tensile) and minimum (compressive) principal strains, corresponding to eight loads, are shown in the Tables 1 and 2.

3.1 Assessment of the correlation between measured versus FE principal strains

The regression analysis between the measured and FE predicted strain data was conducted for both pelvises (Table 3) and scatter plots of the two datasets were generated (Fig. 5). The measured strain (με) was plotted against FE strain (με), for the intact and implanted cases and for all eight loads (Fig. 5). The ideal line, for which measured strain is equal to numerical strain (slope, b = 1.0), was plotted to indicate the quality of agreement (Fig. 5). A strong linear regression was noted between the experiment and FE prediction for both pelvises. In the intact case, the correlation was R = 0.974 (SE = 38.9με). The linear regression slope was b = 1.179 (standard error 2.63%), and the paired t-test demonstrated that this correlation was significant: t-statistic = 38.270, $p < 0.0005$. In the implanted case, the correlation was R = 0.973 (SE = 37.6με). The linear regression slope was b=0.948 (standard error 2.74%), and the paired t-test demonstrated that this correlation was significant: t-statistic = 36.995, $p < 0.0005$.

The Bland-Altman plots for the intact and the implanted pelvises shows limits of agreement between the FE predicted and experimentally measured strains (Fig. 6). The upper and lower limits of agreement for the intact pelvis were 94.43με and – 86.7με, respectively, and the mean value was 3.86με. In the implanted pelvis the mean value, upper and lower limits of agreement were – 6.41με, 68.54με and -81.36με. The concordance correlation coefficient [Lin, 2008] was 0.957 and 0.972 for the intact and the implanted pelvises, respectively. These results indicate that the measured and FE strains are strongly related to each other with a confidence level of more than 95%.

3.2 Comparison of strains: intact versus implanted pelvises

The measured strains before and after implantation were compared (Fig. 7). In the intact case (Table 1), the principal strains were predominantly compressive in rosettes 2, 3 and 5, whereas predominantly tensile strains were measured and predicted for rosette 4. In rosette 1, the tensile and compressive strain magnitudes were similar.

In the implanted pelvis, the same predominant strains were measured and predicted (Table 2, Fig. 7), except for rosette 1, where tensile strain became dominant, largely due to a reduction in compressive strain. After implantation, a reduction of 25%, 33% and 45% in compressive strain magnitude was measured on the lateral cortical surface at rosettes 1, 2 and 3, respectively. Increased compressive strain magnitudes of 123% and 139% were measured on the medial surface at rosettes 4 and 5, respectively. The tensile strains increased at all locations except at rosette 3, where a strain reduction of 68% was measured. The greatest increase in tensile strain of 233% was recorded by rosette 5, located on the medial wall of the pelvis, opposite the acetabulum.

3.3 Implant-bone relative displacement: measured versus FE micromotion

Linear relationships between the implant-bone relative displacements along three orthogonal directions and applied load were observed (Fig. 8), and were compared to predictions from the FE analysis (Fig. 9). The micromotion magnitudes along the medial-lateral and the superior-inferior directions were measured to range from 12 – 30μm and 15 – 27μm, respectively, for applied loads ranging between 700 and 1400 N. Micromotion magnitudes were considerably lower in the anterior-posterior direction, ranging from 1 – 2μm. The FE relative displacement predictions were higher than the measurements, particularly along the medial-lateral direction, ranging between 61 – 85μm. The predicted relative displacements in the superior-inferior direction ranged between 37 – 51μm. However, the FE predicted micromotions in the anterior-posterior direction correlated with the experimental result, ranging between 0.3 – 6μm.

4. Discussion

The purpose of the study was to test the validity of FE models of intact and implanted composite hemi-pelvises, using measurements of bone strain and implant-bone micromotion. Validation of the FE model would demonstrate its suitability for further investigations on the biomechanical performance of the implanted acetabular cup. Although a few studies exist on experimental validation of FE models of the intact pelvis [5, 7, 10] and in-vitro measurement of strains in the implanted pelvis [12–14], there is a lack of studies that attempt to validate both intact and implanted pelvises.

In the present study, the regression analysis (Table 3) indicated a close agreement between the predicted and measured principal strains for both pelvises, with high correlation coefficients (R=0.95-0.98), low SE of the estimates (36-53 με) and low PE in regression slopes (7-11%, Fig. 5). The slope and intercept were not significantly different from 1 and 0, respectively. These results were comparable to those reported in similar studies [5–11, 41, 42]. The Bland-Altman plots and concordance correlation coefficients also showed close agreement between experimentally measured and FE predicted strain. The deviations in FE predictions may be attributed to an effective loss in thickness of the cortex structure in the FE model, arising from CAD model generation or FE meshing. Other reasons for the mismatch in measured and numerical strains could be due to the uncertainty in correlating strain rosette locations and calculating the average FE strain value for a strain rosette location, or both. Despite these minor deviations, the FE model appears to be a valid predictor of actually measured strains in the composite hemi-pelvises.

Compared to the intact pelvis, generally higher tensile strains were recorded in the implanted case, indicating increased load transfer through the cortical shell in locations around the acetabulum. This is evident in the outputs of rosettes 1, 2, 4 and 5 (Tables 1 and 2, Fig. 7), where an increase in tensile strains was observed in the measured and FE predicted values. The compressive and tensile strains in rosettes 4 and 5 increased considerably after implantation, indicating high load transfer through the cortical shell on the rear surface of the acetabulum. However, a reduction in compressive strains for rosettes 1 and 2 was evident, which may not be entirely consistent with increased cortical load transfer observed clinically [43, 44]. In the proximal ilium, a reduction in the tensile and compressive strains was observed in the rosette 3, indicating possible strain shielding. It is therefore evident from the study that implantation causes localised increases in strains in a few locations around the acetabulum. These changes in load transfer mechanism after implantation are corroborated by published data [43–46]. In the clinical study by Wright *et al.* [43], periacetabular bone-mineral density was assessed in a group of twenty-six patients who underwent primary total hip arthroplasty using press-fit acetabular cups. They reported that a greater portion of the load is transmitted through the cup to the peripheral cortex of the acetabulum and the ilium, and consequently, the cancellous bone of the central part of the ilium is mechanically shielded. This was indicated by a decline in retroacetabular bone-mineral density (BMD), which reflected a remodelling response to decreased stress in that region. Furthermore, Laursen *et al.* [44] reported BMD changes that stabilised over the first postoperative year, which is consistent with an adaptive bone remodelling process. The study by Manley *et al.* [46], reported that the implanted pelvis had less load transfer in the anterior and posterior regions of the acetabulum, and adjacent to the ischial facet as compared to the normal hip.

Measured implant-bone relative displacements were found to be low, not exceeding 30 μm, and were in agreement with the trends predicted by the FE results, where the relative displacements were less than 85 μm. Although similar trends were predicted by the FE model, the FE predicted relative displacements along the three orthogonal directions were approximately 2 – 3 times the measured values (Fig. 9). It

should be noted that the measurements of the displacement between the LDS target on the implant and bone included bone deformation. A sensitivity study was carried out by changing the coefficient of friction (μ) between implant-bone, implant-head and cavity-head interfaces. The effect of coefficient of friction between implant-bone (μ = 0.3, 0.4, 0.5 and 0.6) implant-head (μ = 0, 0.005, 0.01 and 0.02) and cavity-head (μ = 0, 0.05, 0.1 and 0.2) interfaces did not influence the implant-bone relative displacements and the strains, similar to earlier published studies [Besong et al., 2001; Udofia et al., 2004; Viceconti et al., 2000].

The magnitude of FE predicted micromotion was considerably greater than the experimental LDS measurements, similar to the results reported by Tarala et al. [2011], Pal et al. [2010], Monti et al. [1999] and Buhler et al. [1997]. Experimental LDS measurements will include both micromotion between the implant and bone, and the deformation of the bone structure between the two reference points of the measurement. Measured micromotion may be higher or lower than FE predicted results, depending on the bone deformation due to bending. Relative displacement calculations from the FE model are not subject to this artefact, and can consider implant-bone micromotion alone. This measurement artefact can be minimized by reducing the distance between the reference point and the measured point [Tarala et al., 2011]. Since the distance between reference point and measured point in our study was 26 mm, the elastic deformation of the bone would lead to deviations from the micromotion measurement. A lower value of measured implant-bone relative displacement, compared to the FE results, indicates that the bone deformation was along the same direction of displacement of the implant due to the applied load, resulting in a net reduction in the measured value of the implant-bone relative displacement. Hence, a careful interpretation of the micromotion results is necessary. Deviations in strain and micromotions could arise elsewhere in the model, for example due to imperfect recreation of the experiment's boundary conditions, such as a change in the position of the hip joint's spherical centre and therefore the load axis. The points of application of load and boundary conditions in the experiment were measured with respect to bony land marks and reproduced in the FE model to within approximately 1mm, but small deviations in FE representation of the applied loading and boundary conditions in the experiment, is another source of error.

This study has a number of limitations. Instead of real bone, a composite bone specimen has been used that possibly cannot reproduce all in-vivo conditions, precisely. However, composite bone has been successfully used in several biomechanical studies, since inter-specimen variability is small and therefore provides more consistency among specimens than cadaveric bone [29–37, 47]. The support structure is still not entirely representative of the in-vivo situation, where there are no rigid constraints. The constraint conditions were carefully designed in an attempt to reproduce a closer representation of physiological support than previous studies [5, 7, 10], which featured large areas of rigid fixation. The use of only five strain rosettes is not enough to draw conclusions on the full field strain distributions in the intact and implanted pelvis. Further experimental study is necessary to obtain more precise data on full field strain distribution to investigate the differences in load transfer due to implantation. Only one loading condition within a normal walking cycle was used, and the action of muscle forces was not included in this model. Quantitative values of the interfacial press-fit and implant-bone friction properties were estimated, but not actually measured, for the FE simulation. The rigid links holding the LDSs were excluded in the FE model; inclusion of thses links and calculating the dispalcement at a'virtual LDS' might result in a more direct comparator between the FE model and the experimental condition. As the purpose of the study was to validate the FE model using a representative analogue experimental model, real bone was not

employed. However, future studies involving bone would have to account for heterogeneity and time dependent behaviour of this complex material.

In conclusion, this study set out to test the validity of FE models of a composite hemi-pelvis, intact and implanted with an acetabular cup. Experimental data was collected which correlated strongly with predictions of surface strains from the FE model, and similar trends were observed between predicted and experimentally measured implant-bone micromotion. This supports the FE model as a valid predictor of the experimentally measured strain in the composite pelvis model, confirming its suitability as a generalised case for further computational investigations, into the understanding of failure mechanisms and the predicted biomechanics of new prosthesis designs.

5. Acknowledgements

The authors sincerely wish to thank UKIERI British Council, Finsbury Orthopaedics Ltd., UK and Department of Biotechnology, New Delhi, for supporting this study. The authors are also thankful for the technical help rendered by Mr. Anton Chitty of Vishay Micro-Measurements, UK.

Declaration of Conflicting interests

The authors hereby declare that with regard to the submission of this article there are no financial or personal relationships with other people and organisations.

References

[1] National Joint Registry for England and Wales, 2009.

[2] Australian National Joint Replacement Registry, 2008, Australian Orthopaedic Association.

[3] Schulte, K.R., Callaghan, J.J., Kelley, S.S., and Johnston, R.C.. The outcome of Charnley total hip arthroplasty with cement after a minimum twenty year follow-up - the results of one surgeon. J. Bone Joint Surg. Am. 1993, 75(9), 961 – 975.

[4] Manley, M.T., Capello, W.N., D'Antonio, J.A., Edidin, A.A., and Geesink, R.G.T. Fixation of acetabular cups without cement in total hip arthroplasty. J. Bone Joint Surg. Am. 1998, 80 (8), 1175 – 1185.

[5] Dalstra, M., Huiskes, R., and van Erning, L. Development and validation of a three dimensional finite element model of the pelvic bone. Trans. ASME, J.Biomech. Eng. 1995, 117(3), 272 – 278.

[6] Gupta, S., van der Helm, F.C.T., Sterk, J.C., van Keulen, F., and Kaptein, B.L. Development and experimental validation of a three dimensional finite element model of the human scapula. Proc. IMechE, Part H: J. Engineering in Medicine 2004, 218(2), 127 – 142.

[7] Anderson, A.E., Peters, C.L., Tuttle, B.D., and Weiss, J.A. Subject-Specific finite element model of the pelvis: development, validation, sensitive studies. Trans. ASME, J. Biomech. Eng. 2005, 127(3), 364 – 373.

[8] Papini, M., Zdero, R., Schemitsch, E.H., and Zalzal., P. The biomechanics of human femurs in axial and torsional loading: comparison of finite element analysis, human cadaveric femurs and synthetic femurs. Trans. ASME, J. Biomech. Eng. 2007. 129 (1), 12 – 19.

[9] Davis, E.T., Olsen, M., Zdero, R., Papini, M., Wadell, J.P., and Schemetisch, E.H. A Biomechanical and Finite Element Analysis of Femoral Neck Notching During Hip Resurfacing. Trans. ASME, J. Biomech. Eng. 2009, 131 (4), (041002)1–8.

[10] Zhang, Q.H., Wang, J.Y., Lupton, C., Adegbile, P.H., Guo, Z.X., Liu, Q., and Tong, J. A subject-specific pelvic bone model and its application to cemented acetabular replacements. J. Biomech. 2010, 43(14), 2722 – 2727.

[11] Pal, B., Gupta, S., New, A.M.R., and Browne, M. Strain and Micromotion in Intact and Resurfaced Composite Femurs: Experimental and Numerical Investigations. J. Biomech. 2010, 43(10), 1923 – 1930.

[12] Lionberger, D., Walker, P.S., and Granholm, J.. Effect of prosthetic acetabular replacement on strains in the pelvis. J. Orthop. Res. 1985, 3(3), 372 – 379.

[13] Miles, A.W., and McNamee, P.B. Strain gauge and photoelastic evaluation of the load transfer in the pelvis in total hip replacement: the effect of the position of the axis of the rotation. Proc. IMechE, Part H: J. Engineering in Medicine 1989, 203(2), 103 – 107.

[14] Massin, P., Vandenbussche, E., Landjerit, B., and Augereau, B. Experimental study of periacetabular deformations before and after implantation of hip prosthesis. J. Biomech. 1996, 29(1), 53 – 61.

[15] Viceconti, M., Brusi, G., Pancanti, A., and Cristofolini, L. Primary stability of an anatomical cementless hip stem: a statistical analysis. J. Biomech. 2006, 39(7), 1169–1179.

[16] Ramamurti, B.S., Orr, T.E., Bragdon, C.R., Lowenstein, J.D., Jasty, M., and Harris, W.H. Factors influencing stability at the interface between a porous surface and cancellous bone: a finite element analysis of a canine in-vivo micromotion experiment. J. Biomed.Materials Res. 1997, 36(2), 274 – 280.

[17] Jasty, M., Bragdon, C., Burke, D., O'Connor, D., Lowenstein, J., and Harris, W. H. In vivo skeletal responses to porous-surfaced implants subjected to small induced motions. J.Bone Joint Surg. Am. 1997, 79(5), 707–714.

[18] Kienapfel, H., Sprey, C., Wilke, A., and Griss, P. Implant fixation by bone ingrowth. J. Arthroplasty 1999, 14(3), 355–368.

[19] Gotze, C., Steens, W., Veith, V., Poremba, C., Claes, L., and Steinback, J. Primary Stability in Cementless Femoral Stems: Custom Made Versus Conventional Femoral Prosthesis. Clin. Biomech. 2002, 17(4), 267 – 273.

[20] Maher, S.A., Prendergast, P.J., and Lyons, C.G. Measurement of migration of a cemented hip prosthesis in an in vitro test. Clin. Biomech. 2001, 16(4), 307 – 314.

[21] Maher, S.A., and Prendergast, P.J. Discriminating the loosening behaviour of cemented hip prostheses using measurement of migration and inducible displacement. J. Biomech. 2002, 35(2), 257 – 267.

[22] Cristofolini, L., Teutonico, S.A., Monti, L., Cappello, A., and Toni, A. Comparetive in vitro study on the long term performance of cemented hip stem: validation of protocol to discriminate between 'good' and 'bad' design. J. Biomech. 2003, 36(11), 1603 – 1615.

[23] Cristofolini, L., Varini, E., and Viceconti, M. In-vitro method for assessing femoral implant-bone micromotions in resurfacing hip implants under different loading conditions. Proc. IMechE, Part H: J. Engineering in Medicine 2007, 221(8), 943 – 950.

[24] Abdul Kadir, M.R., Hansen, U., Klabunde, R., Lucas, D., and Amis, A. Finite element modeling of primary hip stem stability: The effect of interference fit. J. Biomech. 2008, 41(3), 587–594.

[25] Chong, D.Y.R., Hansen, U.N., and Amis, A.A. Analysis of bone-prosthesis interface micromotion for cementless tibial prosthesis fixation and the influence of loading conditions. J. Biomech. 2010, 43(6), 1074 – 1080.

[26] Spears, I.R., Pfleiderer, M., Schneider, E., Hailee, E., Morlock, M.M. The effect of interfacial parameters on cup-bone relative micromotions: a finite element investigation. J. Biomech. 2001, 34(1), 113 – 120.

[27] Ong, K. L., Lehman, J., Notz, W. I., Santner, T. J., and Bartel, D. L. Acetabular cup geometry and bone-implant interface have more influence on initial periprosthetic joint space than joint loading and surgical cup insertion. Trans. ASME, J. Biomech. Eng. 2006, 128(2), 169 – 175.

[28] Janssen, D., Zwartele, R.E., Doets, H.C., Verdonschot, N. Computational assessment of press-fit acetabular implant fixation: the effect of implant design, interference fit, bone quality, and frictional properties. Proc. IMechE, Part H: J. Engineering in Medicine 2010, 224 (H1), 65 – 75.

[29] Stolk, J., Verdonschot, N., Cristofolini, L., Toni, A., and Huiskes, R. Finite element and experimental model of cemented hip joint reconstructions can produce similar bone and cement strains in pre-clinical tests. J. Biomech. 2002, 35(4), 499 – 510.

[30] Waide, D., Cristofolini, L., Stolk., J., Verdonschot, N., and Toni, A. Experimental investigations of bone remodelling using composite femurs. Clin. Biomech. 2003, 18(6), 523 – 536.

[31] Cristofolini, L., Erani, P., Juszczyk, E. B., Ohashi, H., Iida, S., Minato, I., and Viceconti, M. Effect of undersizing on the long-term stability of the Exeter hip stem: A comparative in vitro study. Clin. Biomech. 2010, 25(9), 899 – 908.

[32] Grant, J. A., Bishop, N. E., Gotzen, N., Sprecher, C., Honl, M., and Morlock, M. M. Artificial composite bone as a model of human trabecular bone: The implant bone interface. J. Biomech. 2007, 40(5), 1158 – 1164.

[33] Bolland, B. J. R. F., New, A. M. R., Madabhushi, S. P. G., Oreffo, R. O. C., and Dunlop, D. G. Vibration assisted bone-graft compaction in impaction bone grafting of the femur. J. Bone Jt Surg. Br. 2007, 89(5), 686 – 692.

[34] Bougherara, H., Zdero, R., Mahboob, Z., Dubov, A., Shah, S., and Schemitsch, E. H. The biomechanics of a validated finite element model of stress shielding in a novel hybrid total knee replacement. Proc. IMechE, Part H: J. Engineering in Medicine 2010, 224(H10), 1209 – 1219.

[35] Grover, P., Albert, C., Wang, M., and Harris, G. F. Mechanical characterization of fourth generation composite humerus. Proc. IMechE, Part H: J. Engineering in Medicine 2011, 225(H12), 1169 – 1176.

[36] Kaiser, M. M., Wessel, L. M., Zachert, G., Stratmann, C., Eggert, R., Gros, N., Hessing, M. S., Kienast, B., and Rapp, M. Biomechanical analysis of a synthetic femur spiral fracture model: Influence of different materials on the stiffness in flexible intramedullary nailing. Clin. Biomech. 2011, 26(6), 592 – 597.

[37] Fottner, A., Schmid, M., Birkenmaier, C., Mazoochian, F., Plitz., W., and Jansson, V. Biomechanical evaluation of two types of short-stemmed hip prostheses compared to trust plate prosthesis by three dimensional measurement of micromotion. Clin. Biomech. 2009, 24(5), 429 – 434.

[38] Lewinnek, G.E., Lewis, J.L., Tarr, R., Compere, C.L.,and Zimmerman, J.R. Dislocations after total hip-replacement arthroplasties. J. Bone Joint Surg. Am. 1978, 60 (2), 217 – 220.

[39] Spears, I.R., Pfleiderer, M., Schneider, E., Hailee, E., Bergmann, G., and Morlock, M.M. Interfacial conditions between a press-fit acetabular cup and bone during daily activities: implications for achieving bone in-growth. J. Biomech. 2000, 33(11), 1471 –1477.

[40] Viceconti, M., Muccini, R., Bernakiewicz, M., Baleani, M., and Cristofolini, L. Large-sliding Contact Elements Accurately Predict Levels of Bone-Implant Micromotion Relevant to Osseointegration. J. Biomech. 2000, 33(12), 1611 – 1618.

[41] Taddei, F., Cristofolini, L., Martelli, S., Gill, H.S., and Viceconti, M. Subject-specific finite element models of long bones: An in vitro evaluation of the overall accuracy. J. Biomech. 2006, 39(13), 2457 – 2465.

[42] Schileo, E., Taddei, F., Malandrino, A., Cristofolini, L., and Viceconti, M. Subject specific finite element models can accurately predict strain levels in long bones. J. Biomech. 2007, 40(13), 2982 – 2989.

[43] Wright, J. M., Pellicci, P. M., Salvati, E. A., Ghelman, B., Roberts, M. M., and Koh, J.L. Bone density adjacent to press-fit acetabular components: A prospective analysis with quantitative computer tomography. J. Bone Jt Surg. Am. 2001, 83(4), 529 – 536.

[44] Laursen, M. B., Nielsen, P. T., and Soballe, K. Bone remodeling around HA coated acetabular cup. International Orthopaedics 2007, 31(2), 199 – 204.

[45] Thompson, M.S., Northmore-Ball, M.D., and Tanner, K.E. Effect of acetabular resurfacing component material and fixation on the strain distribution in the pelvis. Proc. IMechE, Part H: J. Engineering in Medicine 2002, 216(H4), 237 – 245.

[46] Manley, M. T., Ong, K. L., and Kurtz, S. M. The potential for bone loss in acetabular structures following THA. Clin. Orthop. Rel. Res. 2006, 453, 246 – 253.

[47] Eberle, S., Gerber, C., von Oldenburg, G., Hogel, F., and Augart, P. A biomechanical evaluation of orthopaedic implants for hip fractures by finite element analysis and in-vitro tests. Proc. IMechE, Part H: J. Engineering in Medicine 2010, 224(H10), 1141 – 1152.

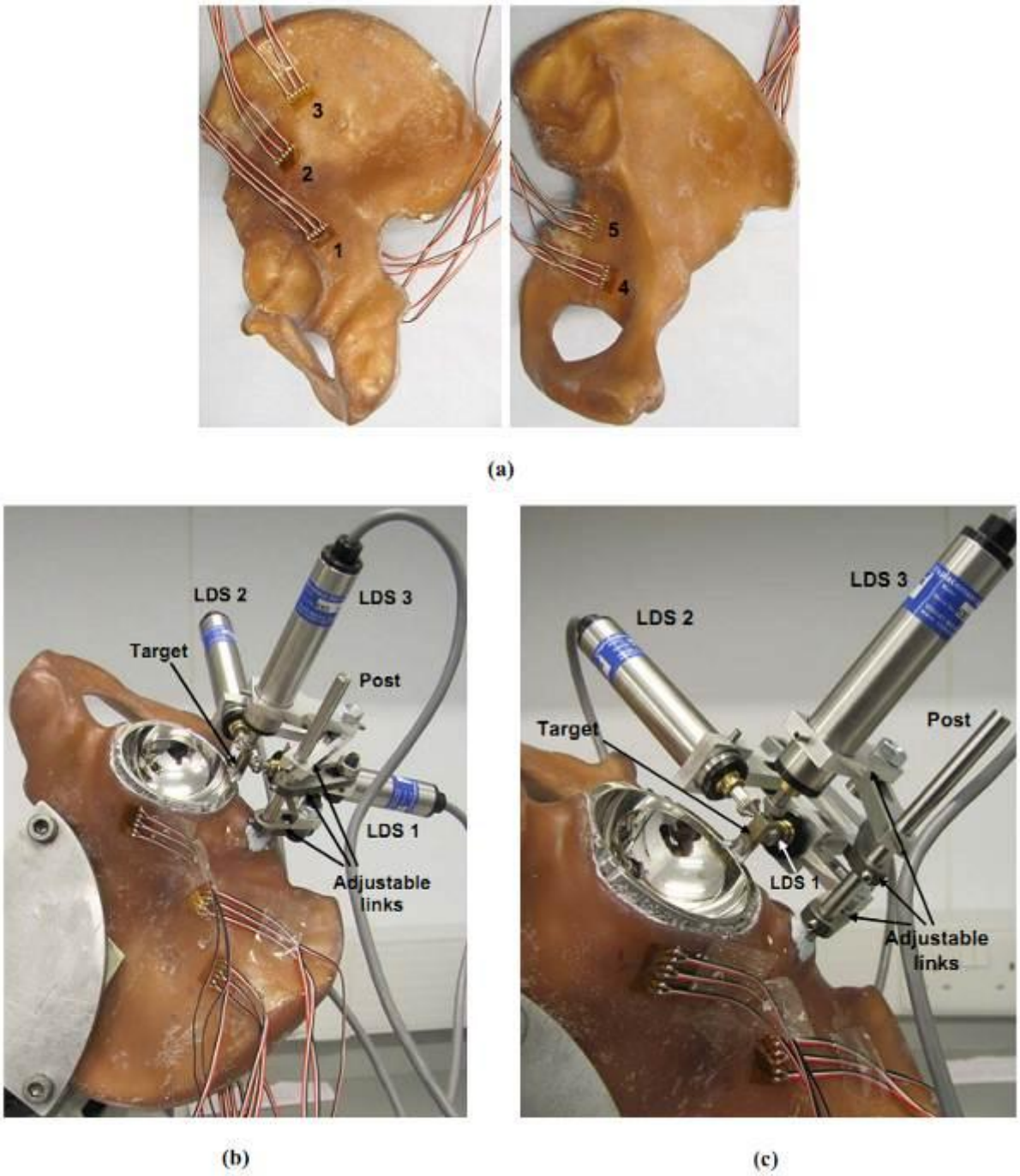

Figure 1. Location of strain rosettes and LDSs mountings in the composite hemi-pelvises: (a) lateral and medial view of strain rosette locations; (b) LDSs mounting, lateral view; (c) LDSs arrangement with target, close-up view.

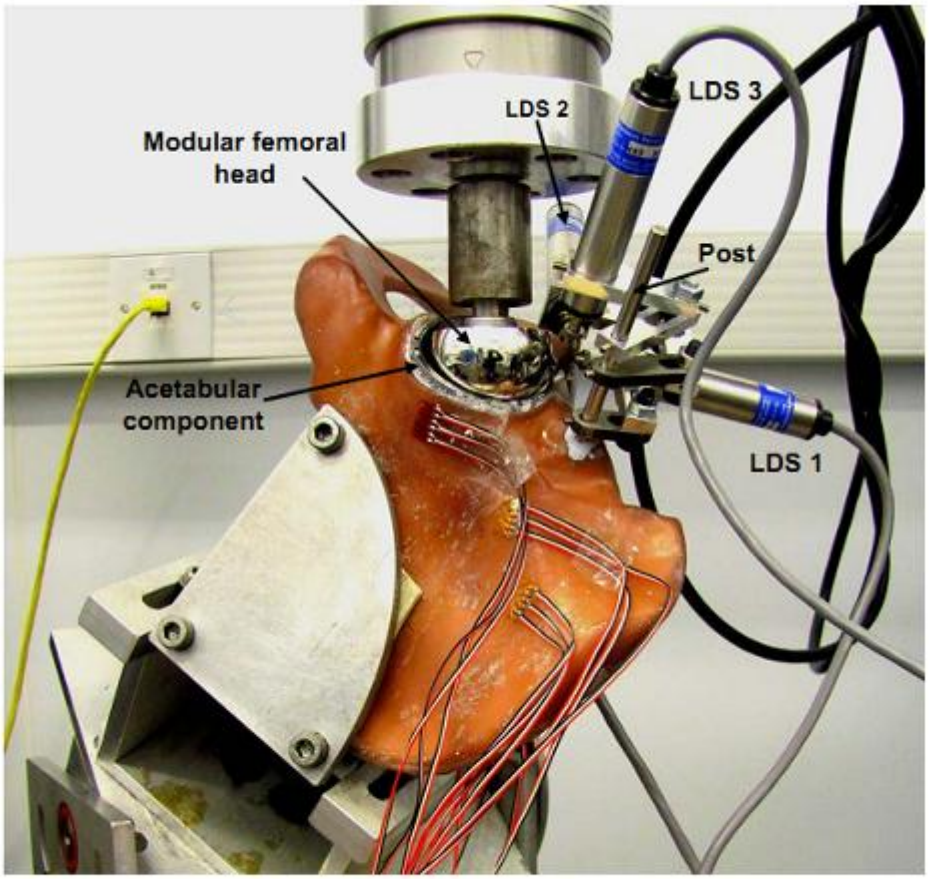

Figure 2. Experimental set-up for strain rosettes and LDSs in the implanted pelvis.

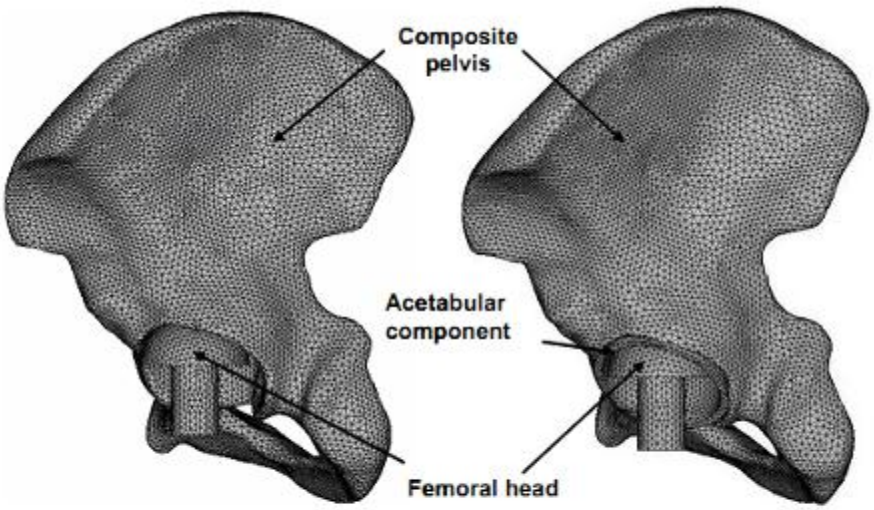

Figure 3. Finite element models of pelvises; (a) intact; (b) implanted.

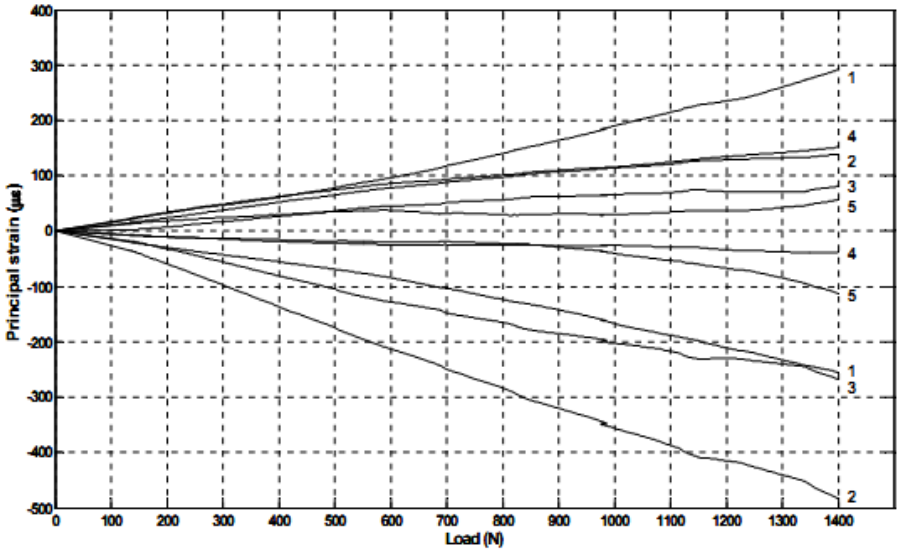

(a)

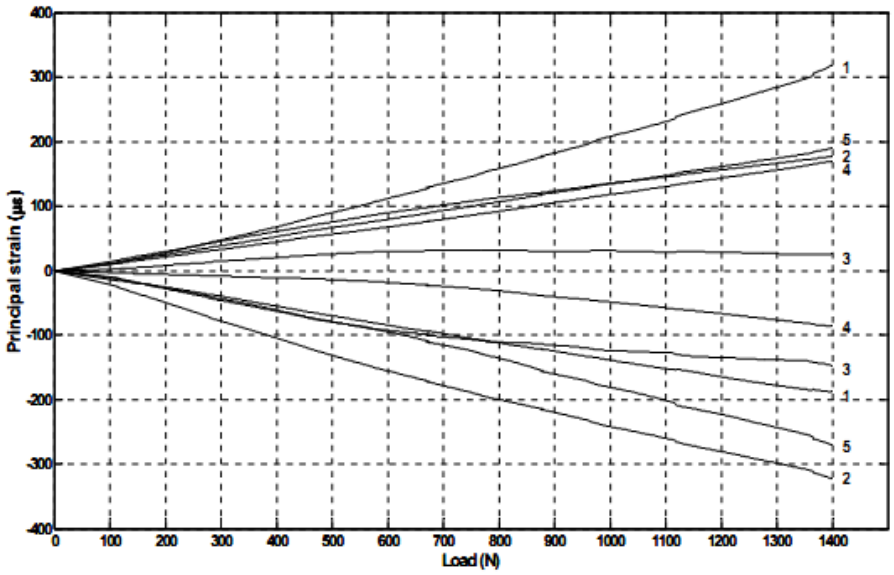

(b)

Figure 4. Principal strains for the five rosettes plotted against applied load: (a) intact hemi-pelvis and (b) implanted hemi-pelvis.

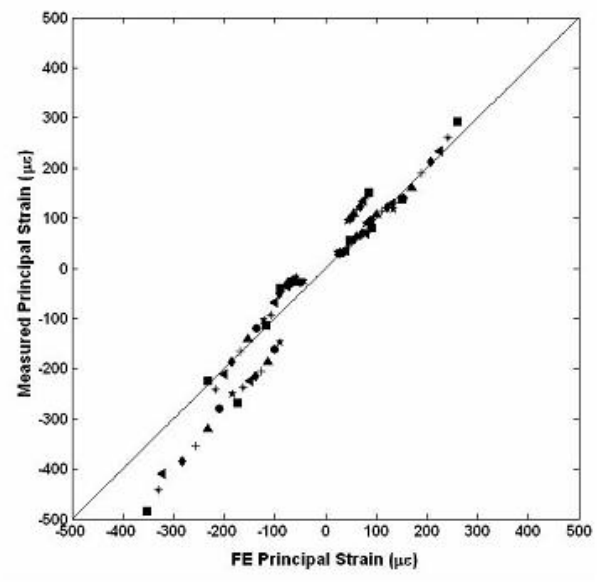

(a)

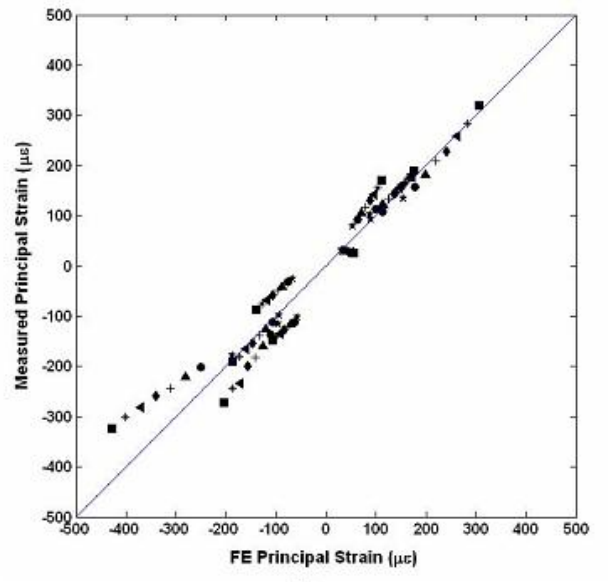

(b)

Figure 5. Measured strain (με) plotted against FE predicted strain (με) with respect to the ideal line (slope = 1, intercept = 0), for all loads, (a) intact; (b) implanted. Markers indicate different loads.

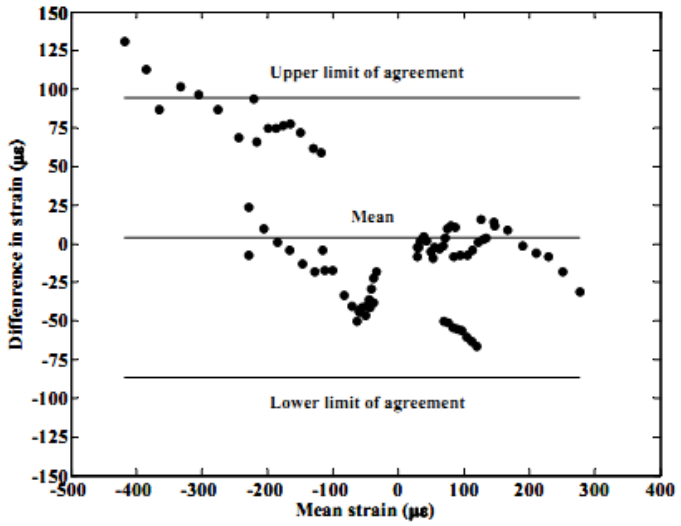

(a)

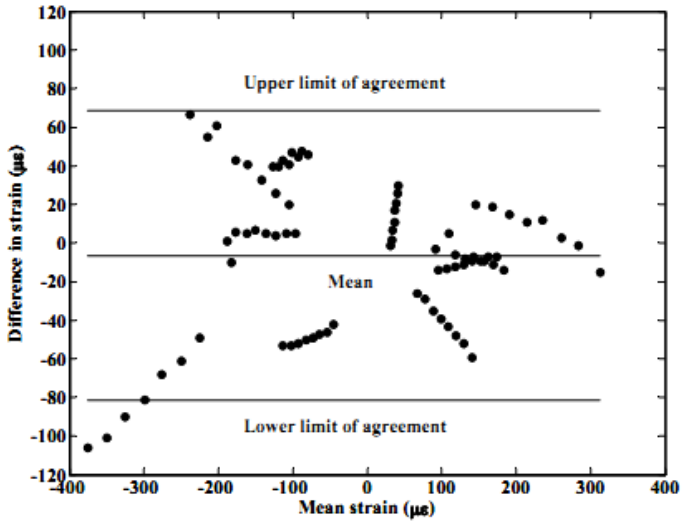

(b)

Figure 6. Bland–Altman plot for agreement between FE predicted strain and experimentally measured strain, with limits of agreement represented by "solid lines". (a) intact pelvis; (b) implanted pelvis.

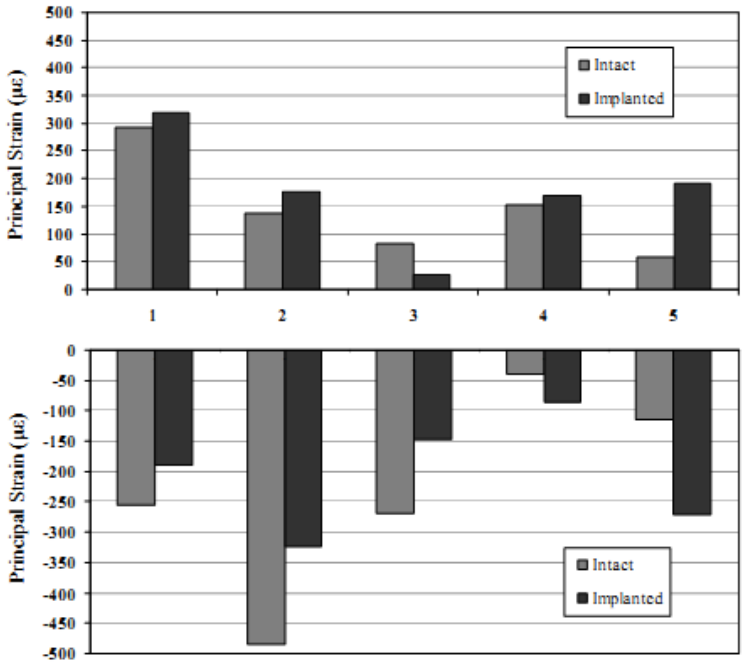

Figure 7. Maximum and Minimum principal strain (με) in the intact and the implanted pelvises at load 1400N. Numbers 1 – 5 on the abscissa indicates strain rosette numbers.

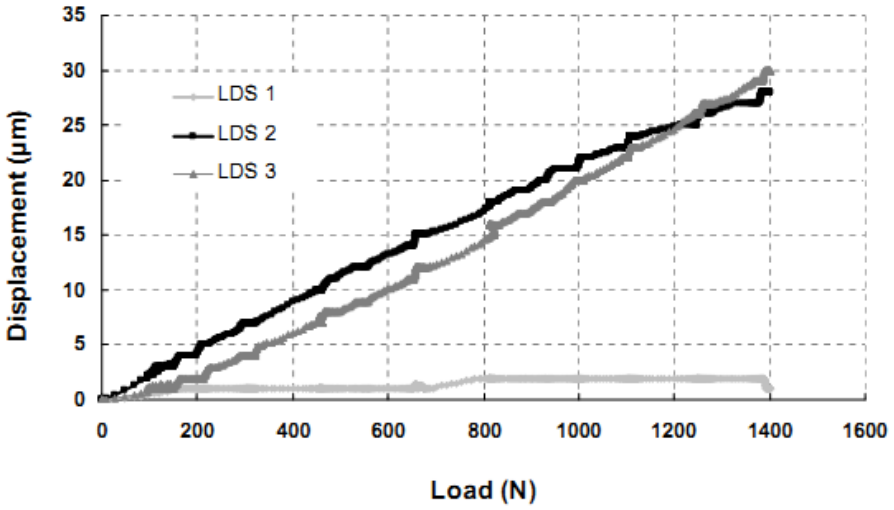

Figure 8. Load versus micromotion curve for the implanted pelvis. Anterior-Posterior (LDS1), Superior-Inferior (LDS2) and Medial-Lateral Direction (LDS3).

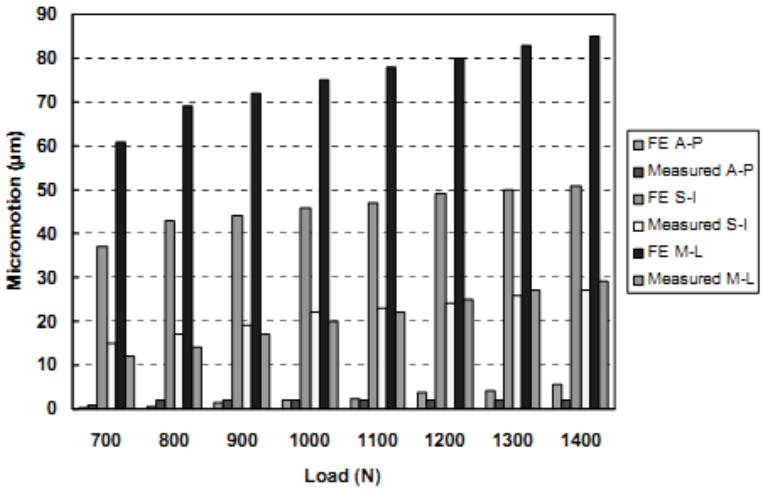

Figure 9. Comparison of implant-bone relative displacements between FE predicted and experimentally measured values. Anterior-posterior (A-P), Superior-Inferior (S-I) and Medial-Lateral directions (M-L).

Table 1. Experimentally measured and FE predicted principal strains (με) for loads 700 – 1400N for the intact pelvis.

		Load															
		700 N		800 N		900 N		1000 N		1100 N		1200 N		1300 N		1400 N	
Strain rosette number	Type of strain	Expt. strain	FE strain	Expt. strain	FE strain	Expt. strain	FE strain	Expt. strain	FE strain	Expt. strain	FE strain	Expt. strain	FE strain	Expt. strain	FE strain	Expt. strain	FE strain
1	Max. principal strain	118	134	141	153	162	171	190	189	213	207	233	225	260	242	292	261
	Min. principal strain	-104	-121	-119	-137	-140	-153	-165	-169	-186	-185	-211	-201	-241	-217	-255	-232
2	Max. principal strain	88	80	97	90	108	101	115	111	121	122	128	131	135	142	138	152
	Min. principal strain	-250	-184	-279	-210	-320	-233	-354	-257	-384	-282	-409	-322	-442	-329	-484	-353
3	Max. principal strain	52	47	56	54	64	61	68	67	69	73	69	79	74	86	81	92
	Min. principal strain	-148	-89	-162	-100	-186	-114	-205	-127	-215	-138	-225	-150	-237	-162	-268	-174
4	Max. principal strain	94	44	101	50	110	56	117	62	124	68	134	74	143	80	152	86
	Min. principal strain	-25	-43	-28	-50	-27	-56	-27	-63	-29	-69	-35	-76	-38	-82	-39	-89
5	Max. principal strain	32	24	29	27	32	30	32	34	34	37	36	41	42	44	57	48
	Min. principal strain	-19	-57	-24	-65	-28	-74	-39	-82	-51	-91	-67	-100	-92	-109	-114	-118

Table 2. Experimentally measured and FE predicted principal strains (με) for loads 700 – 1400N for the implanted pelvis.

		Load															
		700 N		800 N		900 N		1000 N		1100 N		1200 N		1300 N		1400 N	
Strain rosette number	Type of strain	Expt. strain	FE strain	Expt. strain	FE strain	Expt. strain	FE strain	Expt. strain	FE strain	Expt. strain	FE strain	Expt. strain	FE strain	Expt. strain	FE strain	Expt. strain	FE strain
1	Max. principal strain	135	155	158	178	183	199	209	220	229	241	259	263	284	283	320	305
	Min. principal strain	-99	-94	-112	-107	-125	-121	-139	-134	-154	-147	-165	-160	-180	-174	-189	-188
2	Max. principal strain	102	88	113	100	124	112	135	123	145	135	156	147	166	159	177	170
	Min. principal strain	-178	-188	-201	-250	-220	-281	-243	-311	-259	-340	-281	-371	-300	-401	-323	-429
3	Max. principal strain	31	30	32	34	30	38	31	42	28	46	28	50	27	53	26	56
	Min. principal strain	-103	-57	-112	-64	-116	-71	-125	-78	-126	-85	-135	-92	-140	-100	-147	-107
4	Max. principal strain	80	54	92	63	106	70	118	78	130	87	143	95	155	103	170	111
	Min. principal strain	-25	-67	-31	-77	-41	-88	-49	-98	-58	-108	-67	-119	-76	-129	-87	-140
5	Max. principal strain	93	90	107	112	121	114	135	127	146	139	161	151	174	163	190	176
	Min. principal strain	-115	-95	-136	-110	-159	-126	-182	-141	-199	-156	-233	-172	-243	-188	-272	-205

Table 3. Regression analysis of the FE and experimentally measured strain for intact and implanted pelvis for all loads. N is the number of data points.

Load	Strain rosettes and (N)	Correlation coefficient (R)	Standard error (SE) in με	Linear regression y = a + bx		Standard error (SE) of b	Percentage error (SE) of b	t-statistics (P value)
				a	b			
Intact								
700 N	1-5 (N=10)	0.957	36.58	2.848	1.154	0.123	10.65	9.354 (0.000)
800 N	1-5 (N=10)	0.963	38.16	2.639	1.14	0.113	9.91	10.075 (0.000)
900 N	1-5 (N=10)	0.963	43.29	2.106	1.166	0.115	9.86	10.151 (0.000)
1000 N	1-5 (N=10)	0.969	44.47	0.986	1.182	0.107	9.05	11.072 (0.000)
1100 N	1-5 (N=10)	0.973	44.88	-0.076	1.175	0.098	8.36	11.949 (0.000)
1200 N	1-5 (N=10)	0.980	41.82	-0.182	1.151	0.083	7.21	13.877 (0.000)
1300 N	1-5 (N=10)	0.982	43.00	-3.373	1.188	0.081	6.82	14.753 (0.000)
1400 N	1-5 (N=10)	0.982	48.00	-4.31	1.214	0.084	6.92	14.507 (0.000)
All loads	All data(N=80)	0.974	38.913	0.178	1.179	0.031	2.63	38.270 (0.000)
Implanted								
700 N	1-5 (N=10)	0.974	26.65	0.514	1.002	0.083	8.28	12.114 (0.000)
800 N	1-5 (N=10)	0.971	32.15	2.41	0.935	0.082	8.77	11.406 (0.000)
900 N	1-5 (N=10)	0.972	35.16	4.886	0.941	0.08	8.5	11.699 (0.000)
1000 N	1-5 (N=10)	0.973	38.67	4.99	0.947	0.08	8.447	11.887 (0.000)
1100 N	1-5 (N=10)	0.974	41.14	5.89	0.936	0.077	8.226	12.084 (0.000)
1200 N	1-5 (N=10)	0.972	47.32	6.31	0.948	0.082	8.65	11.612 (0.000)
1300 N	1-5 (N=10)	0.974	48.69	8.47	0.943	0.078	8.27	12.137 (0.000)
1400 N	1-5 (N=10)	0.974	53.47	10.57	0.959	0.079	8.24	12.090 (0.000)
All loads	All data(N=80)	0.973	37.60	5.498	0.948	0.026	2.74	36.995 (0.000)